Shock/Gas Bubble Interactions in Infinite and Finite Volumes of Liquid

Nicholas A. HAWKER, Yiannis VENTIKOS*

* Corresponding author: Tel.: +44 1865 283452; Email: Yiannis.Ventikos@eng.ox.ac.uk
Department of Engineering Science, University of Oxford, UK

Abstract: This paper examines the dynamics of shock induced collapse of an air bubble in water and discusses the resulting collapse geometry, pressure and temperature. FronTier, a front tracking algorithm, is used to resolve the motion of the air/water interface. A series of plane shock intensities and bubble sizes are compared and the collapse geometry is found to be independent of these variations. The pressure and temperature are found to be greater for a smaller bubble and for a more intense shock. High speed droplet impact with an enclosed bubble is also examined. The impact creates a shock wave that is found to interact with the bubble in a way largely similar to the plane shock case.

Keywords: Droplet, impact, shock, bubble, interaction

1. Introduction

The interaction of shocks with liquid-gas systems is important in several applications in nature and technology such as shock-wave lithotripsy (Matula et al, 2002), where stones in the body are broken using a focused shock-wave, or in the study of cavitation damage caused by the collapse of bubbles very close to an object (Philipp and Lauterborn, 1998). In this paper, we explore different cases of shock-bubble interaction. A series of shock intensities and bubble sizes are compared and discussed. Moreover, we investigate high-speed droplet impact and study the effects of the intense shocks generated (Haller et al, 2002) on bubbles contained within the droplets.

2. Computational Methodology

The simulations presented here solve the 2D Euler Equations using a front-tracking algorithm (FronTier). The essential feature of this method is that a lower dimensional grid is fitted to and follows the discontinuous shock-waves or fluid-fluid contacts (Glimm et al, 1985). This interface curve or surface has state variables associated with each side and acts as a moving boundary splitting the flow into distinct regions. First the front is advanced using Riemann problem methods, updating the states on the front as well as the position. The hyperbolic equations are then solved using an appropriate hyperbolic solver on the underlying grid, updating the states away from the front. This technique has been shown to perform favorably when compared to a variety of other methods, including the Eulerian level set method, used for computing multi-component flows (Du et al, 2006). In this work front-tracking is used to track the air-water interface of the bubble.

The hyperbolic method used is based on the MUSCL solver (van Leer, 1978) with a limiter applied, as developed by van Leer (van Leer, 1977), to avoid oscillations. Artificial viscosity has been introduced through the use of a slope flattening coefficient.

The equation of state used for air was the ideal gas equation with constants R = 287 and γ = 1.4.

$$p = \rho R T \tag{1}$$

$$e = \frac{p}{\rho(\gamma + 1)} \tag{2}$$

The equation of state used for water was a stiffened polytropic equation,

$$p + (\Gamma + 1)P_\infty = \Gamma p(e + E_\infty) \quad (3)$$

$$c_v \Gamma T = \frac{(p + P_\infty)}{\rho} + \Gamma e_t \rho^\Gamma \quad (4)$$

where the constants are Γ = 4, P_∞ = 6.13e9, c_v = 4180, e_t = 1.11915e-6 and E_∞ = 6.66078e5. Internal energy is taken to be zero at the triple point of water. In both sets of equations p = pressure, T = temperature, ρ = density and e = mass specific internal energy.

3. Results and Discussion

The results presented here examine the collapse mechanism of an air bubble in water and determine the magnitude of the resulting pressure and temperature. First we examine a plane shock wave striking a bubble and then we look at high speed droplet impact.

In the shock-bubble case, a series of observations can be made. Upon shock arrival, the bubble wall begins to move and a strong reflected rarefaction wave is created, as illustrated in Fig. 1. Also, a transmitted shock propagates into the bubble. The pressure rise across this internal shock is weak in comparison to the shock in the water; hence it cannot be seen in Fig. 1. It is much more apparent when looking at the temperature as immediately behind the shock temperatures reach ~3500 K.

As the collapse progresses a large re-entrant jet forms. This then impacts very strongly on the opposite wall causing an outward moving shock wave to be formed. This shock is found to generate pressures 2-3 times higher than those behind the initial shock, as has been seen before by Takahira, Matsuno and Shuto, 2008. The impact shock then passes back through the remains of the, now toroidal, bubble and causes a secondary re-entrant jet to be formed, also illustrated in Fig 1. The passage of this shock highly compresses some regions of the bubble.

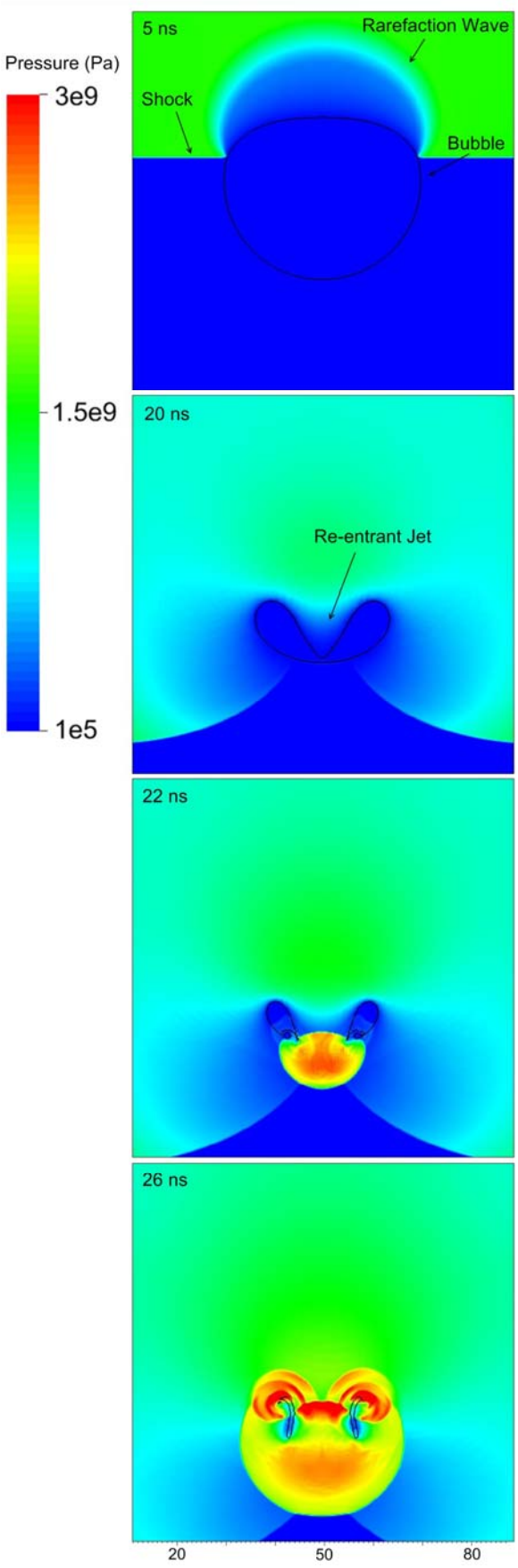

Figure 1: Series of pressure plots for a 40μm bubble in water hit by an M = 1.6 shock. The first pane shows the strong rarefaction, the second the re-entrant jet, the third/fourth the outward shock wave. Times are from first shock bubble contact.

Fig. 3 compares the geometry of collapse for two bubbles of diameter 40 and 10 µm. The difference is minor and both bubbles display the aforementioned characteristics of collapse. However, the time scales do differ with the smaller bubble collapsing in only a quarter of the time (as expected). The faster collapse appears to promote more severe compression in the bubble. The peak pressure and temperature seen in the 40 µm bubble are 4.8 GPa and $8x10^4$ K respectively, whereas in the 10 µm bubble they are 5 GPa and $1x10^5$ K.

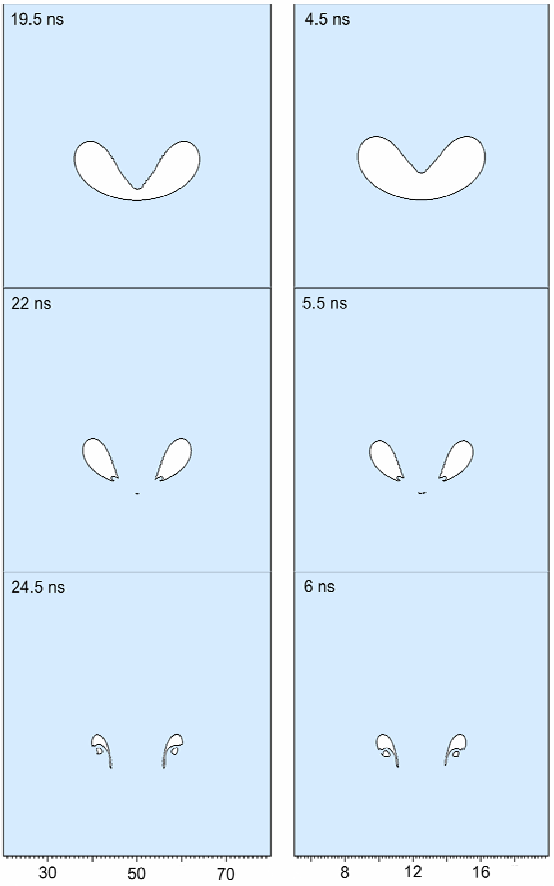

Figure 1: A comparison of the geometry of collapse for 40 µm (left) and 10 µm (right) bubbles. Both are hit by a Mach 1.6 shock and little geometrical difference is seen between the two. Timings are relative to first shock/bubble contact. Distances are µm.

Fig. 4 shows the computational grid used in comparison to the bubble size. Some grid independence studies have been conducted and the geometry is largely unaffected by increased resolution.

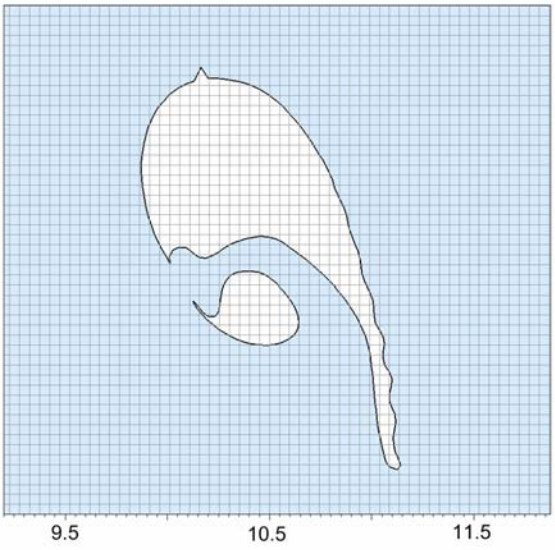

Figure 2: Showing the underlying computation grid and the tracked interface at a late stage of collapse, illustrating the resolution used. Distances are µm.

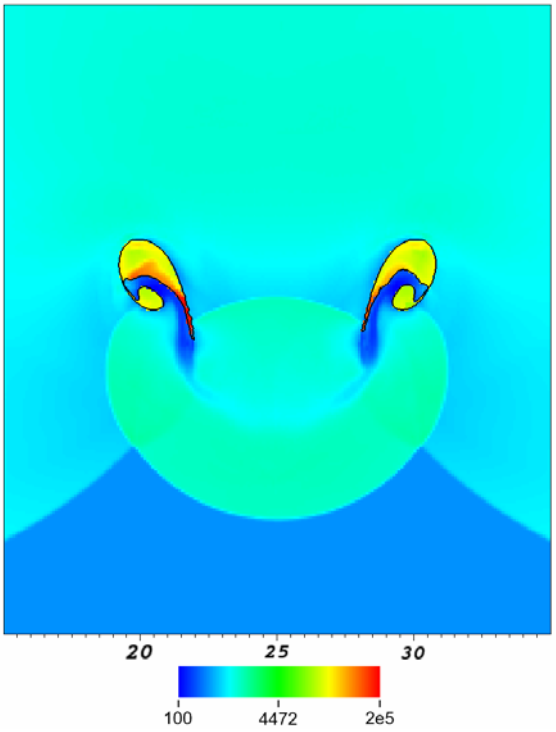

Figure 3: A temperature plot using a log scale to illustrate the location of the highest compression and heating within the bubble collapse. Distances are µm.

Next we compared a Mach 1.2 and a Mach 2 shock wave. The Mach 1.2 shock has a pressure jump of 0.45 GPa whilst the Mach 2 shock has a jump of 3 GPa. Similar to previous

observations, the geometry of collapse didn't appear to change but the time scale and intensity did. The time from first impact of the shock to impact of the first re-entrant jet in the slower case was 21 ns whereas in the fast case it was 7.3 ns. The peak pressure and temperature in the low-intensity shock case are 2 GPa and 3.5×10^4 K respectively, whereas for the high-intensity shock case they are 8 GPa and 1.6×10^5 K. By way of comparison, the temperature predicted to occur during sonoluminescence is roughly an order of magnitude larger (Moss et al, 1994). Fig. 5 shows a plot of the temperature showing where the peak temperature occurs.

Finally we look at high speed droplet impact and the effect of the strong shock wave produced on a bubble within the droplet. Here we model a 160 µm water droplet in air that contains a 40 µm bubble of air. The droplet strikes the wall at 500 ms^{-1} and a shock is created. This shock advances into the bubble and quickly overtakes the contact point, leading to high speed (~6000 ms^{-1}) lateral jetting as observed by Haller et al, 2002. As the shock continues a region of negative pressure develops adjacent to the surface. Pressures reach below -0.2 GPa and would undoubtedly cause significant cavitation in these regions, however the model at its current state of development does not include this capability. At present, they are distant from the region of the bubble and don't seem to influence the collapse. When the shock strikes the bubble the pressure rise is ~0.65 GPa, which gives a plane shock equivalent of a Mach 1.3 wave. Similar to the plane shock case there is a strong reflection off the bubble and a large re-entrant jet is formed. Again, this impacts the opposite side of the bubble and generates a powerful outward shock that compresses the bubble again. This is shown in Fig. 6. The whole process of bubble collapse is very similar to that of the plane shock case.

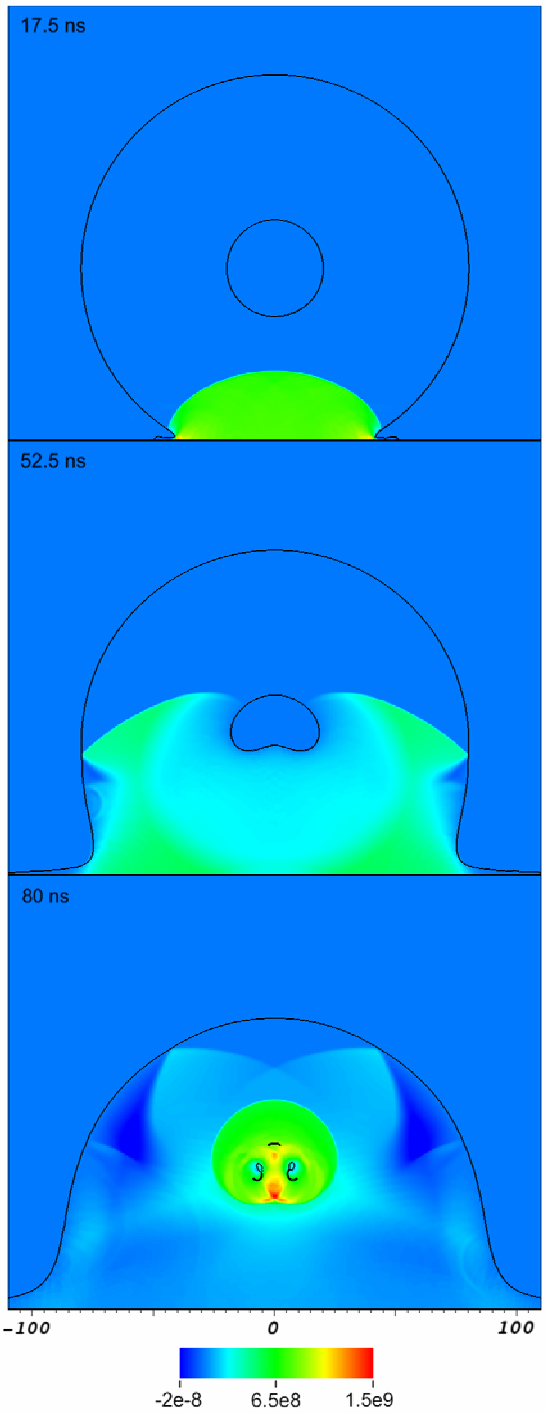

Figure 4: A series of pressure plots showing a 160 µm water droplet containing a 40 µm air bubble striking a wall at 500 ms^{-1}. A shock wave is created that then collapses the bubble. Timing is relative to start of impact. Distances are µm.

4. Conclusions and Future Study

We have investigated the shock induced collapse of a bubble and found that a large re-entrant jet emerges and, upon impact with the far side of the bubble, generates a second shock. This shock causes further re-entrant jetting and compresses the bubble a second time. We have seen that the geometry of collapse is not affected by the size of the bubble. Despite this, in a smaller bubble the pressure and temperature reached is higher than a larger bubble. We have also found that a stronger shock gives rise to greater pressure and temperature even though the geometry is once again very similar. In the case of high speed droplet impact with an entrapped bubble it is found that the bubble collapse is largely similar to the plane shock case. A strong shock is developed by the impact that strikes the bubble and causes collapse.

Future study will involve a move to fully 3D modeling. This may require the use of an adaptive mesh in order to correctly resolve the bubble collapse. The effects of viscosity and surface tension will also be included.

5. References

Du J., Fix B., Glimm J., Jia X.C., Li X.L., Li Y.H., Wu L.L., 2006. A Simple Package for Front Tracking. J. Comp. Phys. 213(2), 613-628

Glimm J., Klingenberg C., Mcbryan O., Plohr B., Sharp D., Yaniv S., 1985. Front Tracking and Two-Dimensional Riemann Problems, Advances in App. Math. 6(3), 259-290

Haller K.K., Ventikos Y., Poulikakos D., Monkewitz P., 2002. Computational Study of High-Speed Liquid Droplet Impact. J. Appl. Phys. 92(5), 2821-2828

Matula T.J., Hilmo P.R., Bailey M.R., Crum L.A., 2002. In Vitro Sonoluminescence and Sonochemistry Studies with an Electrohydraulic Shock-wave Lithotripter. Ultrasound in Med. and Bio. 28(9), 1199-1207.

Moss W.C., Clarke D.B., White J.W., Young D.A., 1994. Hydrodynamic Simulations of Bubble Collapse and Picosecond Sonoluminescence. Phys. Fluids 6, 2979-2985.

Philipp A., Lauterborn W., 1998. Cavitation Erosion by Single Laser Produced Bubbles. J. Fluid Mech. 361, 75-116

Takahira H., Matsuno T., Shuto K., 2008. Numerical investigations of shock–bubble interactions in mercury. Fluid Dynamics Research 40, 510–520.

van Leer B., 1977. Towards the ultimate conservative difference scheme. III - Upstream-centered finite-difference schemes for ideal compressible flow. IV - A new approach to numerical convection. J. Comp. Phys. 23, 263-299.

van Leer B., 1978. Towards the Ultimate Conservative Difference Scheme V. A Second-Order Sequel to Godunov's Method. J. Comp. Phys. 135, 229–248.